ACS OMEGA

http://pubs.acs.org/journal/acsodf

Article

DNA Aptamer-Conjugated Magnetic Graphene Oxide for Pathogenic Bacteria Aggregation: Selective and Enhanced Photothermal Therapy for Effective and Rapid Killing

Muserref A Ocsoy, Sadi Yusufbeyoglu, Nilay Ildiz, Ahmet Ulgen, and Ismail Ocsoy*

Cite This: *ACS Omega* 2021, 6, 20637−20643

Read Online

ACCESS | Metrics & More | Article Recommendations

ABSTRACT: Methicillin-resistant *Staphylococcus aureus* (MRSA), often called "superbug", is a nosocomial and multidrug resistance bacterium that shows resistance to β-lactam antibiotics. There has been high demand to develop an alternative treatment model to antibiotics for efficiently fighting MRSA. Herein, we developed DNA aptamer-conjugated magnetic graphene oxide (Apt@MGO) as a multifunctional and biocompatible nanoplatform for selective and rapid eradication of MRSA and evaluated heat generation and cell death performance of Apt@MGO for the first time under dispersed and aggregated states. The aptamer sequence was specifically selected for MRSA and acted as a molecular targeting probe for selective MRSA recognition and antibiotic-free therapy. Magnetic graphene oxide (MGO) serves as a nanoplatform for aptamer conjugation and as a photothermal agent by converting near-infrared (NIR) light to heat. Iron oxide nanoparticles (Fe_3O_4 NPs) are formed on GO to prepare MGO, which shows magnetic properties for collecting MRSA cells in a certain area in the reaction tube by an external magnet. The collected MGO induces remarkably high local heating and eventual MRSA cell death under NIR laser irradiation. We demonstrate that Apt@MGO resulted in ∼78% MRSA and over >97% MRSA cell inactivation in dispersed and aggregated states, respectively, under 200 seconds (sn) exposure of NIR irradiation (808 nm, 1.1 W cm^{-2}). An in vitro study highlights that Apt@MGO is considered a targeted, biocompatible, and light-activated photothermal agent for efficient and rapid killing of MRSA in the aggregated state under NIR light.

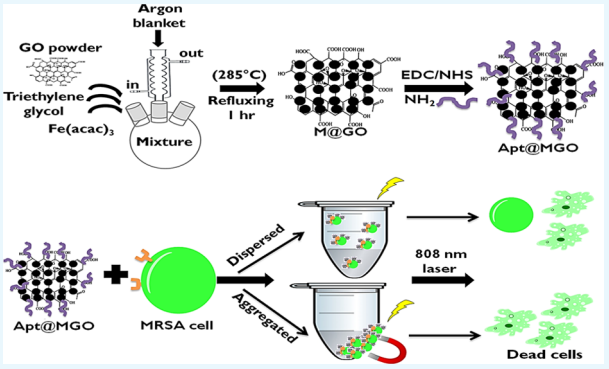

1. INTRODUCTION

Carbon-based nanomaterials,[1] especially graphene oxide (GO),[2,3] carbon nanotube,[4,5] and fullerene,[6] have been dominantly utilized in nanomedicine as versatile tools for the last two decades.[1−6] Among them, graphene oxide (GO) has received considerable attention in biomedicine owing to its biocompatibility, unique physicochemical properties, and stability in biological media.[7,8] In addition, GO has been in use as a therapeutic, drug delivery, and sensing agent, in a variety of biological applications.[9−14] For instance, different metal and metal oxide nanomaterials have been grown or attached on the surface of GO[10−12] used as a great platform to enhance corresponding properties like antimicrobial properties,[13,14] surface-enhanced Raman scattering properties,[10] and so on. In addition, several organic molecules including drugs and photosensitizers have been conjugated on GO to be used in delivery systems, chemo, photodynamic, and photothermal therapies, etc.[15−19] Photothermal therapy (PTT) can be described as a quite simple, noninvasive, controllable, and light-responsive therapy, which potentially serves as an alternative to chemotherapy. The potential mechanism of PTT relies on absorption of light, particularly in the near-infrared (NIR) region by photothermal agents and conversion of NIR light to heat for killing the targets via hyperthermia. Although gold-based nanostructures with certain morphologies (rod, shell, cages, and roses) have been used as effective PTT agents,[20−25] biocompatibility, one-step preparation, and easy functionalization make GO an ideal candidate for PTT.[26−29] However, to provide effective and efficient PTT, active targeting is an indispensable requirement. To date, several targeting ligands including DNA/RNA aptamers, antibodies, RGD peptides, and boronic acids have been actively used for active targeting by researchers.[30−44]

Aptamers composed of DNA or RNA generated by the process called systematic evolution of ligands by exponential

Received: May 31, 2021
Accepted: July 19, 2021
Published: July 29, 2021

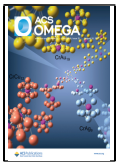

https://doi.org/10.1021/acsomega.1c02832
ACS Omega 2021, 6, 20637−20643

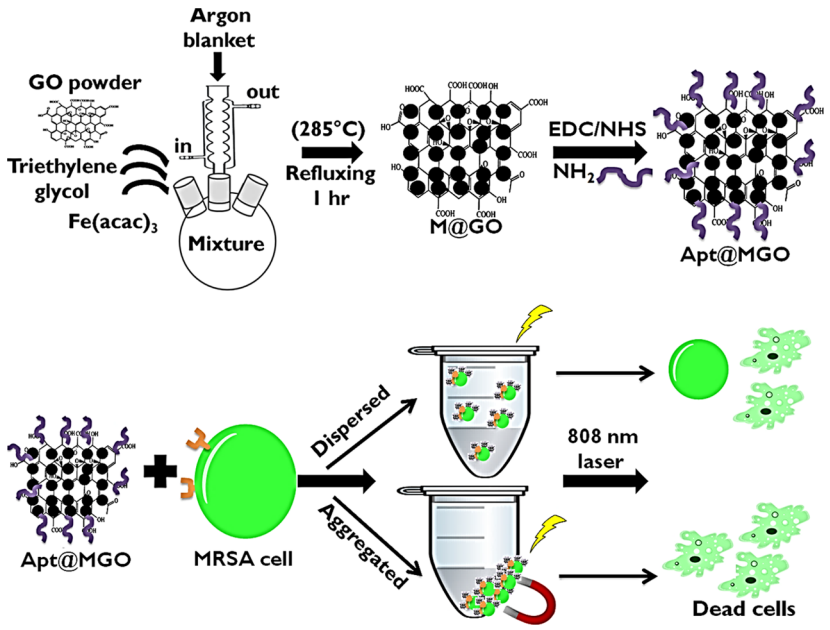

Figure 1. Illustration of preparation of MGO and Apt@MGO, and their PTT performance.

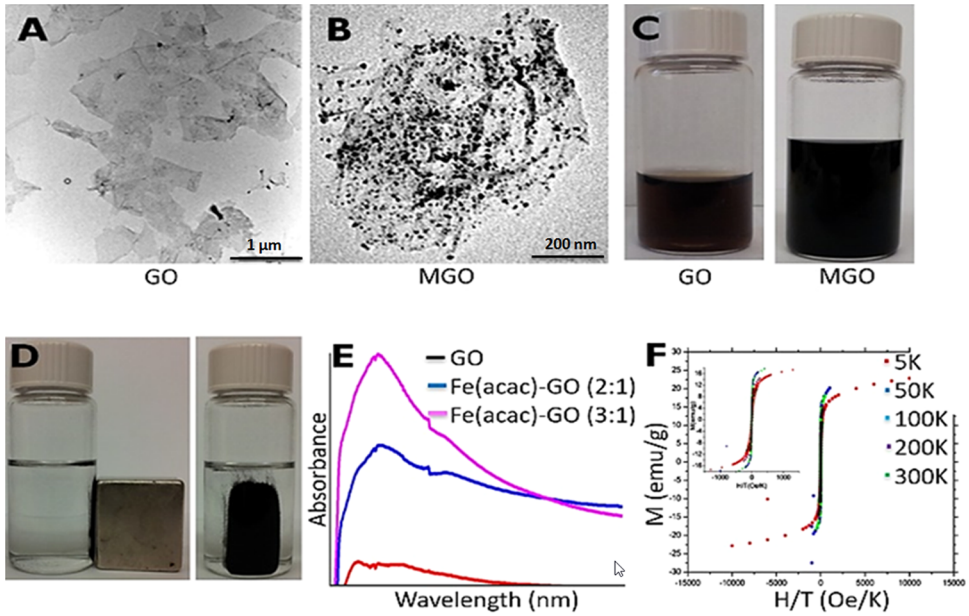

Figure 2. TEM image of (A) bare GO and (B) MGO. (C) Photograph of GO (left) and MGO (right) solutions. (D) Photograph of collected MGO on glass vial with an external magnet. (E) UV−vis spectrum of GO and MGO. (F) Magnetization curve of MGO.

enrichment (SELEX) toward several different targets including metal ions, small molecules, protein, virus, bacteria, and cancer cells have been attractively used.[40−53] Among targeting ligands, aptamers have quite advantages owing to their easy modification with various functional groups, great stability in experimental conditions, and high specificity and affinity (with nanomolar).[54,55]

Herein, we proposed a rational study using DNA aptamer-conjugated magnetic graphene oxide (Apt@MGO) in dispersed and aggregated states for enhanced PTT therapy toward methicillin-resistant *Staphylococcus aureus* (MRSA). First, Apt@MGO specifically binds to the surface of MRSA owing to the targeting function of the aptamer, then Apt@MGO−MRSA cell conjugates are dispersed and aggregated in different reaction tubes, and finally an NIR laser is exposed to each reaction tube for a certain period of time to eradicate MRSA cells through PTT.

2. RESULTS AND DISCUSSION

In this study, Fe_3O_4 nanoparticles (NPs) were formed on the surface of GO by an in vitro process to fabricate magnetic GO (MGO) and utilize their magnetic properties. GO was used as a platform for the growth of Fe_3O_4 NPs and aptamer conjugation and also acted as a PTT agent owing to the conversion of NIR laser irradiation to heat. The role of the aptamer is to provide active targeting by specifically and selectively binding to MRSA cells. Preparation of DNA aptamer-functionalized MGO (Apt@MGO) and its PTT

https://doi.org/10.1021/acsomega.1c02832
ACS Omega 2021, 6, 20637−20643

performance in dispersed and aggregated states are illustrated step by step in Figure 1. In the first step, a certain amount of $Fe(acac)_3$ was added into the GO powder homogeneously dispersed in TREG, and then the mixture was heated to 278 °C to reflux for 60 minutes (min) under an argon blanket and moderate stirring to form MGO. After the successful synthesis of MGO, the second step called DNA aptamer functionalization was carried out. 1-Ethyl-3-(3-dimethylaminopropyl)-carbodiimide/*N*-hydroxy succinimide (EDC/NHS) chemistry was used to activate carboxyl groups (−COOH) present on the edges of GO and to bind the amine ($-NH_2$)-terminated DNA aptamer. In the third step, Apt@MGO bound to MRSA cells and an NIR laser was separately exposed to Apt@MGO−MRSA cell conjugates in dispersed and aggregated states.

In terms of characterization, morphologies of bare GO and MGO were monitored by transmission electron microscopy (TEM) images shown in Figure 2A,B, respectively. While the size of Fe_3O_4 NPs grown on the surface of GO was measured to be ∼11 nm, the density of Fe_3O_4 NPs on GO was arranged with weight ratios of $Fe(acac)_3$ and GO powder as fixed $Fe(acac)_3$/GO (2:1). The original brown color of GO (left) and black color of MGO (right) solutions are shown in Figure 2C. The magnetic properties of MGO dispersed in the phosphate-buffered saline (PBS) solution were tested using an external magnet, as shown in Figure 2D. As seen that MGO was collected at the wall of a glass vial in the presence of a magnet, which can be an indication of the magnetic response of MGO. The absorbance points of GO (red line) and MGO (blue and pink lines) were determined to be ∼240 and ∼285 nm, respectively (Figure 2E). The magnetization curve of MGO was generated at various temperatures (5, 50, 100, 200, and 300 K, Figure 2F). While magnetization reached saturation at low temperatures, the superparamagnetic behavior of MGO was observed at high temperatures and even above the blocking temperature. In addition, the zero field-cooled (ZFC) magnetization increases with increasing temperature until the blocking temperature.

The heat generation performances of MGO when dispersed and aggregated in the PBS buffer under 808 nm NIR laser irradiation were tested. Three different concentrations of MGO in each state were prepared and exposed to the corresponding laser irradiation for 200 seconds (sn) as shown in Figure 3. While 10 ppm (green line), 50 ppm (blue line), and 100 ppm (red line) MGO in the dispersed state increased the temperature of reaction solutions from ∼24 to ∼37, ∼39, and ∼48 °C, respectively, under 60 sn NIR laser exposure (Figure 3A), MGO with same concentrations and experimental conditions in the aggregated state caused a dramatic temperature increase in the localized reaction area from ∼24 to ∼38, ∼43, and ∼54 °C, respectively (Figure 3B). We claim that aggregation of MGO in the restricted area by an external magnet caused effective heat generation in the reaction medium with efficient and rapid absorption of the photon energy of NIR. The results also show that 50 and 100 ppm MGO in the aggregated state can both be considered as ideal concentrations for hyperthermia in PTT compared to the dispersed state.

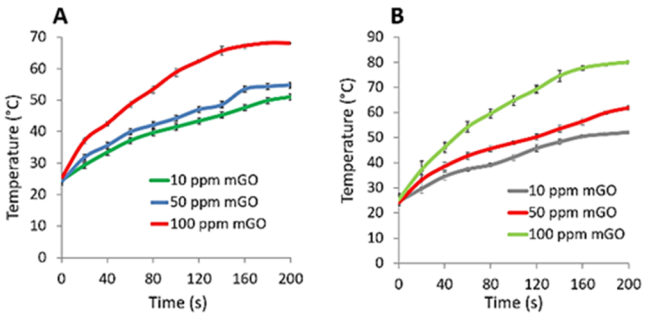

Figure 3. Heat production performance of MGO with different concentrations. (A) 10 ppm (green line), 50 ppm (blue line), and 100 ppm (red line) MGO in the dispersed state and (B) 10 ppm (gray line), 50 ppm (red line), and 100 ppm (green line) MGO in the aggregated state under a continuous wave laser (808 nm) with a power density of 1.1 W cm^{-2} for 200 sn.

The molecular recognition of Apt@MGO was monitored with flow cytometric analysis in Figure 4. Simply, the MRSA aptamer, random DNA sequence (cDNA)-conjugated MGO (cDNA@MGO), and MRSA aptamer DNA sequence-conjugated MGO (Apt@MGO) were separately incubated with MRSA cells in PBS buffer (concentration around 10^7 CFU/mL) at 37 °C for 1 h. After incubation, reaction tubes containing the MRSA aptamer and MRSA cells were washed with PBS buffer by centrifugation; however, the reaction tubes containing MGO were washed without centrifugation by collecting MGO−MRSA cell conjugates with a magnet. The flow cytometry study showed that only the MRSA cell suspension did not give any fluorescence signal (red lien) as expected. Although cDNA was labeled with fluorescein isothiocyanate (FTIC) dye, no fluorescence signal was observed with cDNA@MGO (blue line) to show its binding to MRSA cells. The reason is that cDNA is composed of random sequences and used as nonspecific and nonselective control sequences for MRSA cells. In contrast, the MRSA aptamer (brown line) and Apt@MGO (purple line) gave strong fluorescence signals with the right shift, which are an indication of their selective and specific binding to the surface of MRSA cells. As a further study, the selective and specific binding capability of the aptamer for MRSA cells was tested with *Enterococcus faecalis* cells used as control cells. The aptamer did not bind to *E. faecalis* cells (green line) as expected.

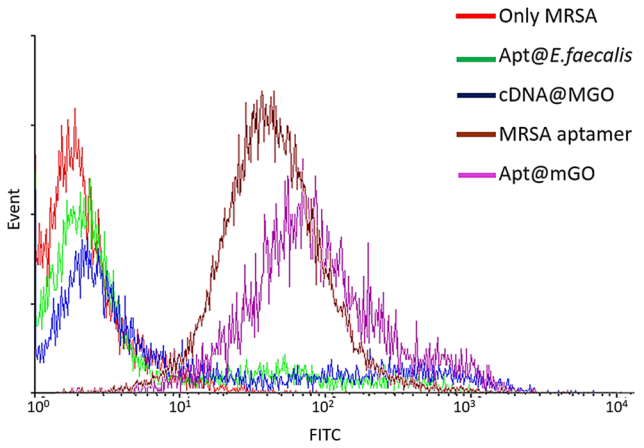

Figure 4. Flow cytometry results for showing the binding of aptamer sequences to MRSA cells.

The TEM images show the morphologies of MRSA cells with well-defined and deformed structures (Figure 5). The round-shaped MRSA cell and its cell division are demonstrated

https://doi.org/10.1021/acsomega.1c02832
ACS Omega 2021, 6, 20637−20643

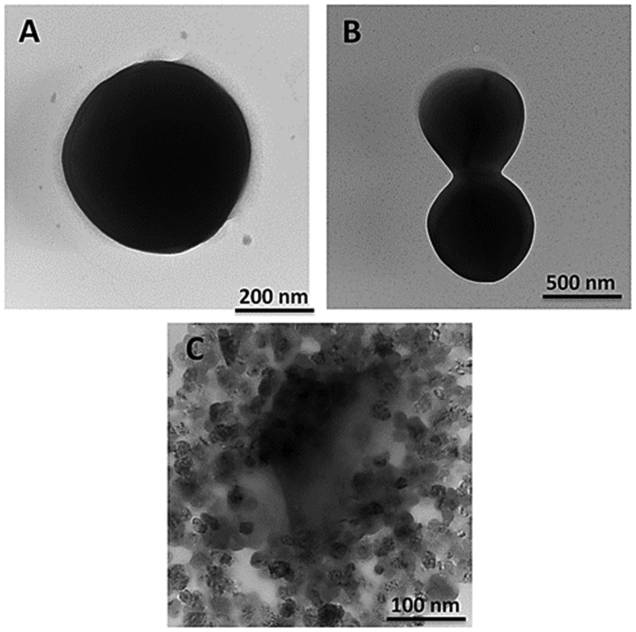

Figure 5. TEM images of the MRSA cell (A, B) before and (C) after PTT.

in Figure 5A,B, respectively, before PTT. However, destruction of the MRSA cell with hypothermia in PTT is monitored in Figure 5C. The MRSA cell lost its rigid and intact membrane and rapidly turned into debris in a minute.

The PTT performance of MGO in dispersed and aggregated states is demonstrated in Figure 6. As expected, the aptamer

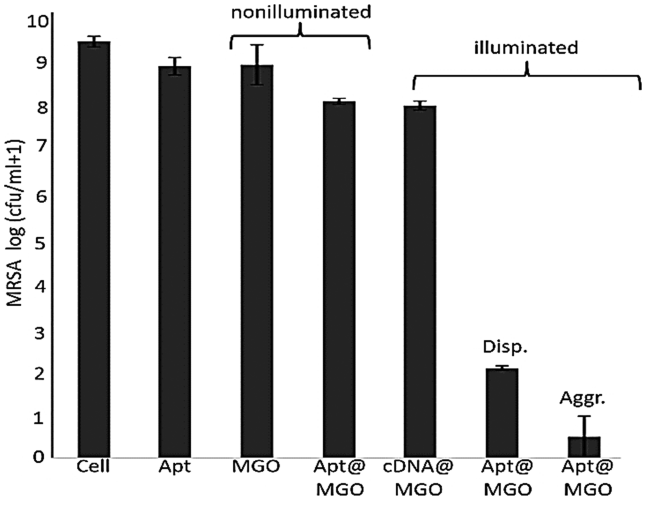

Figure 6. MRSA Cell viability test under nonilluminated and illuminated conditions when using MGO in dispersed and aggregated states.

itself did not cause any cell activation when incubated with MRSA cells. In addition, MGO and Apt@MGO also did not inactivate an acceptable amount of MRSA cells under no NIR laser illumination. It is worthy to mention that although Apt@MGO specifically bound to MRSA cells, no MRSA cell was killed owing to two potential reasons: (i) MGO was not able to generate heat without NIR laser exposure and (ii) MGO is quite biocompatible. Additionally, the PTT performance of MGO was also studied under illumination conditions. cDNA@MGO displayed around 12% cell reduction owing to nonspecific adsorption of a very less number of MGO to MRSA cells. However, Apt@MGO effectively killed MRSA cells. While Apt@MGO in the dispersed state resulted in around 78% of cells in 200 sn, more than 95% of MRSA cells were killed when Apt@MGO was used in the aggregated state. We proposed that Apt@MGO in the aggregated state efficiently and rapidly adsorbed the NIR laser and turned it into high heat in the local area, which caused a drastic increase in cell death.

For PTT, we designed a custom-made NIR laser system composed of an 808 nm 10 watt F-mount laser diode, as shown in Figure 7.

Figure 7. Custom-made NIR laser system composed of an 808 nm 10 watt F-mount laser diode.

3. CONCLUSIONS

In summary, we developed a biocompatible, targeted, and PTT agent called Apt@MGO and used it in the aggregated form for the effective, rapid, and efficient killing of MRSA cells under NIR laser irradiation. The MRSA aptamer selectively captured the MRSA cells, and MGO acted as a multifunctional nanoplatform for aptamer functionalization and Fe_3O_4 NP growth and also as a PTT agent. We demonstrated that MGO generated much more heat under NIR laser exposure in the aggregated state compared to the dispersed state. Then, rapid destruction of MRSA cells in a short time was implemented. We proposed that Apt@MGO can be a promising targeted and PTT agent owing to its targeting and biocompatible properties and provides extraordinary heat production in the aggregated form.

4. EXPERIMENTAL SECTION

4.1. Materials and Methods. Graphene oxide was obtained from Graphene Supermarket (Ronkonkoma, NY). Triethylene glycol (TREG), iron(III) acetylacetonate ($Fe(acac)_3$), 1-ethyl-3-(3-dimethylaminopropyl)carbodiimide (EDC), *N*-hydroxy succinimide (NHS), and metal salts (NaCl, KCl, Na_2HPO_4, KH_2PO_4, $CaCl_2.2H_2O$, and $MgCl_2.6H_2O$) for the preparation of phosphate-buffered saline (PBS) were purchased from Sigma-Aldrich. For the preparation of the aptamer, all nucleotides including phosphoramidites and 5′-amino and 3′-FITC modifiers were purchased from

https://doi.org/10.1021/acsomega.1c02832
ACS Omega 2021, 6, 20637−20643

Glen Research (Sterling, VA). MRSA standard strain 43 300 was obtained from Erciyes University, Faculty of Pharmacy, Pharmaceutical Microbiology research laboratory. Copper grids were purchased from Electron Microscopy Sciences. Deionized (DI) water (18.2 MΩ·cm) was used in all experiments. All chemicals were used as received without further purification. In terms of characterization, the concentration of aptamers and absorbance points of GO and MGO were determined using an 1800 UV−vis spectrophotometer (Shimadzu Scientific Instruments, Columbia, MD). The images of GO, MGO, and MRSA cells were obtained using a transmission electron microscope (TEM, a Hitachi H-700 TEM instrument with a working voltage of 100 kV). A superconducting quantum interference device (SQUID) was used for the measurement of the magnetic properties of MGO. The DNA MRSA aptamer was synthesized with a DNA/RNA synthesizer (ABI3400 DNA/RNA synthesizer, Applied Biosystems, Foster City, CA). The DNA sequences were purified by high-pressure liquid chromatography (HPLC, ProStar instrument, Varian, Walnut Creek, CA) with a reverse phase C-18 column (Econosil, 5u, 250 × 4.6 mm) from Alltech (Deerfield, IL). PTT was carried using a custom-made NIR laser system (continuous wave laser with an 808 nm wavelength and 1.1 W cm^{-2} optical power density).

4.2. Synthesis of Aptamers. The selected MRSA DNA aptamer sequences [5′-FITC-ATC CAG ACG TGA CGC AGC $(N)_{38}$ TGG ACA CGG TGG CTT AGTA-NH_2−3′, $(N)_{38}$ = ATG CGG TTG GTT GCG GTT GGG CAT GAT GTA TTT CTGTG] were synthesized at a 1 μmol scale. After synthesis, the sequences were deprotected using a standard protocol. Typically, the sequences were incubated in a mixture of 40% ammonium hydroxide (NH_4OH) and methylamine (CH_3NH_2) 1:1 at 65 °C for 30 min prior to HPLC operation for purification. After that, the sequences were lyophilized and then dispersed in DI water for the measurement of their absorbances to calculate their concentrations.

4.3. Preparation of Magnetic Graphene Oxide (MGO). MGO was synthesized using a reported method.[56] GO powder (20 mg) was dispersed in 20 mL of triethylene glycol (TREG), and then it was sonicated until a black color solution was obtained, which is an indication of homogeneous dispersion of GO in TREG. After that, 20 mg of $Fe(acac)_3$ was added into a 100 mL glass flask containing 20 mL of TREG, and then the resulting mixture was vigorously stirred and refluxed at 278 °C for 50 minutes (min) under an argon blanket. After refluxing, the mixture was cooled down to room temperature (25 °C). The mixture was washed with ethanol by centrifugation at 10 000 rpm for 10 min; the washing process was repeated three times to remove excess solvent and unreacted components. The product, MGO, was collected and dried in vacuum and then stored for further characterization and application.

4.4. Preparation of DNA Aptamer-Functionalized MGO. We utilized protein labeling chemistry for the functionalization of MGO with the MRSA aptamer. A 50 μL aliquot of 0.1 M 1-ethyl-3-(3-dimethylaminopropyl)-carbodiimide (EDC) was added into 150 mg mL^{-1} MGO in the PBS solution (10 mM, pH 7.4), and then the mixture was gently mixed for 30 min to activate the carboxyl groups present at the edges of MGO. After shaking for 30 min, a 20 μL aliquot of 0.12 M *N*-hydroxy succinimide (NHS) and a 20 μL aliquot of 250 μM MRSA aptamer solutions were sequentially injected into the mixture above. Then, the final mixture was shaken continuously for 4 hours (hr) for covalently binding the aptamer to MGO. The washing step was completed by magnetically separating Apt@MGO using an external magnet. Thus, excess and nonspecific binding aptamer was removed by decantation of the supernatant. The final product, Apt@MGO, was dispersed in PBS and stored at 4 °C for further PTT application.

4.5. Bacteria Strains and Bacteria Culture. MRSA was cultured using a standard protocol (ATCC medium 18-Trypticase soy agar overnight at 37 °C) prior to photothermal experiments. After the MRSA culture process, the MRSA concentration (10^7 CFU/mL, OD_{600}) was adjusted in 10% PBS.

The photothermal therapy (PTT) performance of MGO for PTT, 10^7 CFU/mL MRSA cells suspended in solution were used. One hundred micrograms of MGO, random DNA-functionalized Au NPs and MGO, and MRSA Apt@MGO were separately mixed with the bacteria solution and each mixture was incubated for 30 min at 37 °C. After incubation, the mixture of Apt@MGO and MRSA cells was divided into two sets, and then the PTT performance of Apt@GO in dispersed and aggregated states under NIR laser irradiation (a single-mode (sm) 808 nm NIR laser with a power of 1.1 W cm^{2-}) was determined. In addition, the effect of illumination and no illumination of the NIR laser on the mixtures was studied.

AUTHOR INFORMATION

Corresponding Author

Ismail Ocsoy − *Department of Analytical Chemistry, Faculty of Pharmacy, Erciyes University, 38039 Kayseri, Turkey;* orcid.org/0000-0002-5991-3934; Email: ismailocsoy@erciyes.edu.tr

Authors

Muserref A Ocsoy − *Department of Physics, Faculty of Science, Erciyes University, 38039 Kayseri, Turkey*

Sadi Yusufbeyoglu − *Department of Analytical Chemistry, Faculty of Pharmacy, Erciyes University, 38039 Kayseri, Turkey; Department of Pharmacognosy, Faculty of Gülhane Pharmacy, University of Health Sciences, 06010 Ankara, Turkey*

Nilay Ildiz − *Department of Pharmaceutical Microbiology, Faculty of Pharmacy, Erciyes University, 38039 Kayseri, Turkey*

Ahmet Ulgen − *Department of Chemistry, Faculty of Science, Erciyes University, 38039 Kayseri, Turkey*

Complete contact information is available at: https://pubs.acs.org/10.1021/acsomega.1c02832

Author Contributions

M.A.O. performed all experiments and was involved in manuscript writing as a first author. S.Y., N.I, and A.U. also contributed to experiments and manuscript writing. I.O. conceived the original idea, supervised the project, and wrote and revised the manuscript.

Funding

This work was supported by grants from the Erciyes University Scientific Research Office (FDA-2017-6980 and FYL-2018-8132) and a grant from The Scientific and Technological Research Council of Turkey TUBITAK (215Z572).

Notes

The authors declare no competing financial interest.

https://doi.org/10.1021/acsomega.1c02832
ACS Omega 2021, 6, 20637−20643

■ ACKNOWLEDGMENTS

The authors thank Ulgen Lab for the custom-made NIR laser system. The authors would like to thank Mucahit Osman Turkan and Busra Aydin for their assistance in drawing and designing the front cover.

■ ABBREVIATIONS USED

MRSA, methicillin-resistant *Staphylococcus aureus*; GO, graphene oxide; MGO, magnetic graphene oxide; DNA@MGO, DNA aptamer-conjugated magnetic graphene oxide; cDNA, random DNA sequence; cDNA@MGO, cDNA-conjugated MGO; NIR, near-infrared region; PTT, photothermal therapy; sm, single mode; SELEX, systematic evolution of ligands by exponential enrichment; TREG, triethylene glycol; $Fe(acac)_3$, iron (III) acetylacetonate; EDC, 1-ethyl-3-(3-dimethylaminopropyl)carbodiimide; NHS, *N*-hydroxy succinimide; PBS, phosphate-buffered saline; SQUID, superconducting quantum interference device; HPLC, high-pressure liquid chromatography; min, minutes; sn, seconds; hr, hour

■ REFERENCES

(1) Cha, C.; Shin, S. R.; Annabi, N.; Dokmeci, M. R.; Khademhosseini, A. Carbon-Based Nanomaterials: Multifunctional Materials for Biomedical Engineering. *ACS Nano* **2013**, *7*, 2891−2897.

(2) Georgakilas, V.; Tiwari, J. N.; Kemp, K. C.; Perman, J. A.; Bourlinos, A. B.; Kim, K. S.; Zboril, R. Noncovalent Functionalization of Graphene and Graphene Oxide for Energy Materials, Biosensing, Catalytic, and Biomedical Applications. *Chem. Rev.* **2016**, *116*, 5464−5519.

(3) Chung, C.; Kim, Y.-K.; Shin, D.; Ryoo, S.-R.; Hong, B. H.; Min, D.-H. Biomedical Applications of Graphene and Graphene Oxide. *Acc. Chem. Res.* **2013**, *46*, 2211−2224.

(4) Shi, X.; Wang, S. H.; Shen, M.; Antwerp, M. E.; Chen, X.; Li, C.; Petersen, E. J.; Huang, Q.; Weber, W. J.; Baker, J. R. Multifunctional Dendrimer-Modified Multiwalled Carbon Nanotubes: Synthesis, Characterization, and In Vitro Cancer Cell Targeting and Imaging. *Biomacromolecules* **2009**, *10*, 1744−1750.

(5) Alshehri, R.; Ilyas, A. M.; Hasan, A.; Arnaout, A.; Ahmed, F.; Memic, A. Carbon Nanotubes in Biomedical Applications: Factors, Mechanisms, and Remedies of Toxicity. *J. Med. Chem.* **2016**, *59*, 8149−8167.

(6) Castro, E.; Garcia, A. H.; Zavala, G.; Echegoyen, L. Fullerenes in Biology and Medicine. *J. Mater. Chem. B* **2017**, *5*, 6523−6535.

(7) Gu, D.; Zhou, Y.; Ma, R.; Wang, F.; Liu, Q.; Wang, J. Facile Synthesis of N-Doped Graphene-Like Carbon Nanoflakes as Efficient and Stable Electrocatalysts for the Oxygen Reduction Reaction. *Nano-Micro Lett.* **2018**, *10*, No. 29.

(8) Pinto, A. M.; Gonçalves, I. C.; Magalhães, F. D. Graphene-Based Materials Biocompatibility: A Review. *Colloids Surf., B* **2013**, *111*, 188−202.

(9) Zhang, A.; Chang, J.; Chen, Y.; Huang, Z.; Alfranca, G.; Zhang, Q.; Cui, D. Spontaneous Implantation of Gold Nanoparticles on Graphene Oxide for Salivary SERS Sensing. *Anal. Methods* **2019**, *11*, 5089−5097.

(10) Li, Z.; Jiang, S.; Huo, Y.; Ning, T.; Liu, A.; Zhang, C.; He, Y.; Wang, M.; Li, C.; Man, B. 3D Silver Nanoparticles with Multilayer Graphene Oxide as a Spacer for Surface Enhanced Raman Spectroscopy Analysis. *Nanoscale* **2018**, *10*, 5897−5905.

(11) Ocsoy, I.; Gulbakan, B.; Chen, T.; Zhu, G.; Chen, Z.; Sari, M. M.; Peng, L.; Xiong, X.; Fang, X.; Tan, W. DNA-Guided Metal-Nanoparticle Formation on Graphene Oxide Surface. *Adv. Mater.* **2013**, *25*, 2319−2325.

(12) Strayer, A.; Ocsoy, I.; Tan, W.; Jones, J. B.; Paret, M. L. Low Concentrations of a Silver-Based Nanocomposite to Manage Bacterial Spot of Tomato in the Greenhouse. *Plant Dis.* **2016**, *100*, 1460−1465.

(13) Ocsoy, I.; Paret, M. L.; Ocsoy, M. A.; Kunwar, S.; Chen, T.; You, M.; Tan, W. Nanotechnology in Plant Disease Management: DNA-Directed Silver Nanoparticles on Graphene Oxide as an Antibacterial Against Xanthomonas Perforans. *ACS Nano* **2013**, *7*, 8972−8980.

(14) Ocsoy, I.; Temiz, M.; Celik, C.; Altinsoy, B.; Yilmaz, V.; Duman, F. A Green Approach for Formation of Silver Nanoparticles on Magnetic Graphene Oxide and Highly Effective Antimicrobial Activity and Reusability. *J. Mol. Liq.* **2017**, *227*, 147−152.

(15) Tian, B.; Wang, C.; Zhang, S.; Feng, L.; Liu, Z. Photothermally Enhanced Photodynamic Therapy Delivered by Nano-Graphene Oxide. *ACS Nano* **2011**, *5*, 7000−7009.

(16) Ocsoy, I.; Isiklan, N.; Cansiz, S.; Özdemir, N.; Tan, W. ICG-Conjugated Magnetic Graphene Oxide for Dual Photothermal and Photodynamic Therapy. *RSC Adv.* **2016**, *6*, 30285−30292.

(17) Deb, A.; Vimala, R. Camptothecin Loaded Graphene Oxide Nanoparticle Functionalized with Polyethylene Glycol and Folic Acid for Anticancer Drug Delivery. *J. Drug Delivery Sci. Technol.* **2018**, *43*, 333−342.

(18) Koninti, R. K.; Sengupta, A.; Gavvala, K.; Ballav, N.; Hazra, P. Loading of an Anti-Cancer Drug onto Graphene Oxide and Subsequent Release to DNA/RNA: A Direct Optical Detection. *Nanoscale* **2014**, *6*, 2937−2944.

(19) Pei, X.; Zhu, Z.; Gan, Z.; Chen, J.; Zhang, X.; Cheng, X.; Wan, Q.; Wang, J. PEGylated Nano-Graphene Oxide as a Nanocarrier for Delivering Mixed Anticancer Drugs to Improve Anticancer Activity. *Sci. Rep.* **2020**, *10*, No. 2717.

(20) Li, C.; Chen, T.; Ocsoy, I.; Zhu, G.; Yasun, E.; You, M.; Wu, C.; Zheng, J.; Song, E.; Huang, C. Z.; Tan, W. Gold-Coated Fe_3O_4 Nanoroses with Five Unique Functions for Cancer Cell Targeting, Imaging, and Therapy. *Adv. Funct. Mater.* **2014**, *24*, 1772−1780.

(21) Greenwell, H. C.; Lloyd-Evans, M.; Wenner, C. Biofuels, Science and Society. *Interface Focus* **2013**, *3*, No. 20120093.

(22) Huang, Y.-F.; Sefah, K.; Bamrungsap, S.; Chang, H.-T.; Tan, W. Selective Photothermal Therapy for Mixed Cancer Cells Using Aptamer-Conjugated Nanorods. *Langmuir* **2008**, *24*, 11860−11865.

(23) Ocsoy, I.; Yusufbeyoglu, S.; Yılmaz, V.; Mclamore, E. S.; Ildız, N.; Ülgen, A. DNA Aptamer Functionalized Gold Nanostructures for Molecular Recognition and Photothermal Inactivation of Methicillin-Resistant *Staphylococcus Aureus*. *Colloids Surf., B* **2017**, *159*, 16−22.

(24) Bardhan, R.; Lal, S.; Joshi, A.; Halas, N. J. Theranostic Nanoshells: From Probe Design to Imaging and Treatment of Cancer. *Acc. Chem. Res.* **2011**, *44*, 936−946.

(25) Au, L.; Zheng, D.; Zhou, F.; Li, Z.-Y.; Li, X.; Xia, Y. A Quantitative Study on the Photothermal Effect of Immuno Gold Nanocages Targeted to Breast Cancer Cells. *ACS Nano* **2008**, *2*, 1645−1652.

(26) Wang, Y.-W.; Fu, Y.-Y.; Peng, Q.; Guo, S.-S.; Liu, G.; Li, J.; Yang, H.-H.; Chen, G.-N. Dye-Enhanced Graphene Oxide for Photothermal Therapy and Photoacoustic Imaging. *J. Mater. Chem. B* **2013**, *1*, No. 5762.

(27) Li, J.-L.; Hou, X.-L.; Bao, H.-C.; Sun, L.; Tang, B.; Wang, J.-F.; Wang, X.-G.; Gu, M. Graphene Oxide Nanoparticles for Enhanced Photothermal Cancer Cell Therapy under the Irradiation of a Femtosecond Laser Beam. *J. Biomed. Mater. Res., Part A* **2014**, *102*, 2181−2188.

(28) Yan, M.; Liu, Y.; Zhu, X.; Wang, X.; Liu, L.; Sun, H.; Wang, C.; Kong, D.; Ma, G. Nanoscale Reduced Graphene Oxide-Mediated Photothermal Therapy Together with IDO Inhibition and PD-L1 Blockade Synergistically Promote Antitumor Immunity. *ACS Appl. Mater. Interfaces* **2019**, *11*, 1876−1885.

(29) Tang, Z.; Shangguan, D.; Wang, K.; Shi, H.; Sefah, K.; Mallikratchy, P.; Chen, H. W.; Li, Y.; Tan, W. Selection of Aptamers for Molecular Recognition and Characterization of Cancer Cells. *Anal. Chem.* **2007**, *79*, 4900−4907.

(30) Kausaite-Minkstimiene, A.; Ramanaviciene, A.; Kirlyte, J.; Ramanavicius, A. Comparative Study of Random and Oriented Antibody Immobilization Techniques on the Binding Capacity of Immunosensor. *Anal. Chem.* **2010**, *82*, 6401−6408.

https://doi.org/10.1021/acsomega.1c02832
ACS Omega 2021, 6, 20637−20643

(31) Shangguan, D.; Li, Y.; Tang, Z.; Cao, Z. C.; Chen, H. W.; Mallikaratchy, P.; Sefah, K.; Yang, C. J.; Tan, W. Aptamers Evolved from Live Cells as Effective Molecular Probes for Cancer Study. *Proc. Natl. Acad. Sci. U.S.A.* **2006**, *103*, 11838−11843.
(32) Qiu, L.; Chen, T.; Öçsoy, I.; Yasun, E.; Wu, C.; Zhu, G.; You, M.; Han, D.; Jiang, J.; Yu, R.; Tan, W. A Cell-Targeted, Size-Photocontrollable, Nuclear-Uptake Nanodrug Delivery System for Drug-Resistant Cancer Therapy. *Nano Lett.* **2015**, *15*, 457−463.
(33) Zhang, Y.; Chen, Y.; Han, D.; Ocsoy, I.; Tan, W. Aptamers Selected by Cell-SELEX for Application in Cancer Studies. *Bioanalysis* **2010**, *2*, 907−918.
(34) Gandioso, A.; Cano, M.; Massaguer, A.; Marchán, V. A Green Light-Triggerable RGD Peptide for Photocontrolled Targeted Drug Delivery: Synthesis and Photolysis Studies. *J. Org. Chem.* **2016**, *81*, 11556−11564.
(35) Liu, Z.; Chen, K.; Davis, C.; Sherlock, S.; Cao, Q.; Chen, X.; Dai, H. Drug Delivery with Carbon Nanotubes for In Vivo Cancer Treatment. *Cancer Res.* **2008**, *68*, 6652−6660.
(36) Tajima, N.; Takai, M.; Ishihara, K. Significance of Antibody Orientation Unraveled: Well-Oriented Antibodies Recorded High Binding Affinity. *Anal. Chem.* **2011**, *83*, 1969−1976.
(37) Deshayes, S.; Cabral, H.; Ishii, T.; Miura, Y.; Kobayashi, S.; Yamashita, T.; Matsumoto, A.; Miyahara, Y.; Nishiyama, N.; Kataoka, K. Phenylboronic Acid-Installed Polymeric Micelles for Targeting Sialylated Epitopes in Solid Tumors. *J. Am. Chem. Soc.* **2013**, *135*, 15501−15507.
(38) Khan, T.; Igarashi, K.; Tanabe, A.; Miyazawa, T.; Fukushima, S.; Miura, Y.; Matsumoto, Y.; Yamasoba, T.; Matsumoto, A.; Cabral, H.; Kataoka, K. Structural Control of Boronic Acid Ligands Enhances Intratumoral Targeting of Sialic Acid to Eradicate Cancer Stem-like Cells. *ACS Appl. Bio Mater.* **2020**, *3*, 5030−5039.
(39) Karaagac, Z.; Onal, I.; Ildiz, N.; Ocsoy, I. Simultaneous Use of Phenylboronic Acid as a Phase Transfer Agent and Targeting Ligand for Gold Nanoparticles. *Mater. Lett.* **2020**, *280*, No. 128561.
(40) Karaagac, Z.; Yusufbeyoglu, S.; iIldiz, I.; Sellami, H.; Ocsoy, I. A Facile and One-PotAqueous Phase Transfer of Oleylamine Capped Au NP with Aminophenylboronic Acid Used as Transfer and Targeting Ligand. *Enzyme Microb. Technol.* **2021**, *148*, No. 109810.
(41) Hong, C.; Zhang, X.; Ye, S.; Yang, H.; Huang, Z.; Yang, D.; Cai, R.; Tan, W. Aptamer-Pendant DNA Tetrahedron Nanostructure Probe for Ultrasensitive Detection of Tetracycline by Coupling Target-Triggered Rolling Circle Amplification. *ACS Appl. Mater. Interfaces* **2021**, *13*, 19695−19700.
(42) Cai, R.; Du, Y.; Yang, D.; Jia, G.; Zhu, B.; Chen, B.; Lyu, Y.; Chen, K.; Chen, D.; Chen, W.; Yang, L.; Zhao, Y.; Chen, Z.; Tan, W. Free-Standing 2D Nanorafts by Assembly of 1D Nanorods for Biomolecule Sensing. *Nanoscale* **2019**, *11*, 12169−12176.
(43) Chen, X.; Qiu, L.; Cai, R.; Cui, C.; Li, L.; Jiang, J.-H.; Tan, W. Aptamer-Directed Protein-Specific Multiple Modifications of Membrane Glycoproteins on Living Cells. *ACS Appl. Mater. Interfaces* **2020**, *12*, 37845−37850.
(44) Zhou, X.; Duan, R.; Xing, D. Highly Sensitive Detection of Protein and Small Molecules Based on Aptamer-Modified Electrochemiluminescence Nanoprobe. *Analyst* **2012**, *137*, No. 1963.
(45) Ocsoy, I.; Gulbakan, B.; Shukoor, M. I.; Xiong, X.; Chen, T.; Powell, D. H.; Tan, W. Aptamer-Conjugated Multifunctional Nanoflowers as a Platform for Targeting, Capture, and Detection in Laser Desorption Ionization Mass Spectrometry. *ACS Nano* **2013**, *7*, 417−427.
(46) Yasun, E.; Gulbakan, B.; Ocsoy, I.; Yuan, Q.; Shukoor, M. I.; Li, C.; Tan, W. Enrichment and Detection of Rare Proteins with Aptamer-Conjugated Gold Nanorods. *Anal. Chem.* **2012**, *84*, 6008−6015.
(47) Miao, X.; Ling, L.; Shuai, X. Ultrasensitive Detection of Lead (II) with DNAzyme and Gold Nanoparticles Probes by Using a Dynamic Light Scattering Technique. *Chem. Commun.* **2011**, *47*, No. 4192.
(48) Turek, D. Molecular Recognition of Live Methicillin-Resistant *Staphylococcus aureus* Cells Using DNA Aptamers. *World J. Transl. Med.* **2013**, *2*, 67−74.
(49) Shukoor, M. I.; Altman, M. O.; Han, D.; Bayrac, A. T.; Ocsoy, I.; Zhu, Z.; Tan, W. Aptamer-Nanoparticle Assembly for Logic-Based Detection. *ACS Appl. Mater. Interfaces* **2012**, *4*, 3007−3011.
(50) Chen, T.; Öçsoy, I.; Yuan, Q.; Wang, R.; You, M.; Zhao, Z.; Song, E.; Zhang, X.; Tan, W. One-Step Facile Surface Engineering of Hydrophobic Nanocrystals with Designer Molecular Recognition. *J. Am. Chem. Soc.* **2012**, *134*, 13164−13167.
(51) Le, T. T.; Adamiak, B.; Benton, D. J.; Johnson, C. J.; Sharma, S.; Fenton, R.; Mccauley, J. W.; Iqbal, M.; Cass, A. E. G. Aptamer-Based Biosensors for the Rapid Visual Detection of Flu Viruses. *Chem. Commun.* **2014**, *50*, 15533−15536.
(52) Ocsoy, I.; Ocsoy, M. A.; Yasun, E.; Tan, W. Nucleic Acid-Functionalized Nanomaterials. *Nano LIFE* **2013**, *03*, No. 1340004.
(53) Wang, J.; Zhu, G.; You, M.; Song, E.; Shukoor, M. I.; Zhang, K.; Altman, M. B.; Chen, Y.; Zhu, Z.; Huang, C. Z.; Tan, W. Assembly of Aptamer Switch Probes and Photosensitizer on Gold Nanorods for Targeted Photothermal and Photodynamic Cancer Therapy. *ACS Nano* **2012**, *6*, 5070−5077.
(54) Bamrungsap, S.; Chen, T.; Shukoor, M. I.; Chen, Z.; Sefah, K.; Chen, Y.; Tan, W. Pattern Recognition of Cancer Cells Using Aptamer-Conjugated Magnetic Nanoparticles. *ACS Nano* **2012**, *6*, 3974−3981.
(55) Fan, Z.; Shelton, M.; Singh, A. K.; Senapati, D.; Khan, S. A.; Ray, P. C. Multifunctional Plasmonic Shell−Magnetic Core Nanoparticles for Targeted Diagnostics, Isolation, and Photothermal Destruction of Tumor Cells. *ACS Nano* **2012**, *6*, 1065−1073.
(56) Cong, H. P.; He, J. J.; Lu, Y.; Yu, S. H. Water-Soluble Magnetic-Functionalized Reduced Graphene Oxide Sheets: In situ Synthesis and Magnetic Resonance Imaging Applications. *Small* **2010**, *6*, 169−173.

https://doi.org/10.1021/acsomega.1c02832
ACS Omega 2021, 6, 20637−20643